Cell Death and Differentiation (2011) 18, 191–200

www.nature.com/cdd

Dendritic spine loss and neurodegeneration is rescued by Rab11 in models of Huntington's disease

P Richards[1], C Didszun[1], S Campesan[2], A Simpson[1], B Horley[1], KW Young[1], P Glynn[1], K Cain[1], CP Kyriacou[2], F Giorgini[2] and P Nicotera*[,1,3]

Huntington's disease (HD) is a fatal neurodegenerative disorder caused by expansion of a polyglutamine tract in the huntingtin protein (htt) that mediates formation of intracellular protein aggregates. In the brains of HD patients and HD transgenic mice, accumulation of protein aggregates has been causally linked to lesions in axo-dendritic and synaptic compartments. Here we show that dendritic spines – sites of synaptogenesis – are lost in the proximity of htt aggregates because of functional defects in local endosomal recycling mediated by the Rab11 protein. Impaired exit from recycling endosomes (RE) and association of endocytosed protein with intracellular structures containing htt aggregates was demonstrated in cultured hippocampal neurons cells expressing a mutant htt fragment. Dendrites in hippocampal neurons became dystrophic around enlarged amphisome-like structures positive for Rab11, LC3 and mutant htt aggregates. Furthermore, Rab11 overexpression rescues neurodegeneration and dramatically extends lifespan in a *Drosophila* model of HD. Our findings are consistent with the model that mutant htt aggregation increases local autophagic activity, thereby sequestering Rab11 and diverting spine-forming cargo from RE into enlarged amphisomes. This mechanism may contribute to the toxicity caused by protein misfolding found in a number of neurodegenerative diseases.
Cell Death and Differentiation (2011) **18,** 191–200; doi:10.1038/cdd.2010.127; published online 19 November 2010

Huntington's disease (HD) is a fatal neurodegenerative disease caused by expansion of a polyglutamine (polyQ) tract in the huntingtin protein (htt).[1] The expansion of this polyQ region beyond a critical threshold of ~35 glutamines leads to formation of insoluble intranuclear and cytoplasmic amyloid fibers resulting from self-association of mutant htt.[2] Mutant htt-containing aggregates have been identified in the brains of HD patients,[3] as well as in mice expressing mutant htt.[4] Critically, polyQ length in mutant htt correlates directly with the kinetics of its aggregation *in vitro* and as well as with disease severity.[5,6]

Although protein aggregates are a consistent feature of many neurodegenerative diseases,[7] their role in the degenerative process is unclear. Although several studies have found aggregates to be associated with cell death,[8–10] others have found no correlation between aggregation of mutant htt and cellular toxicity.[11,12,13] A provocative study has found that the presence of inclusion bodies containing mutant htt may actually predict lower risk of cell death in primary neurons.[14] Indeed, it has been DZNE, German Center for Neurodegenerative Diseases, suggested that htt aggregates may represent a molecular sink for soluble toxic htt forms.[11,14] Recent work indicates that soluble oligomers or 'micro-aggregates' of mutant htt, which may represent one of the toxic species of misfolded htt critical for HD pathology, form in a polyQ-dependent manner both *in vitro* and *in vivo*.[15] Such soluble aggregate species precede symptoms in HD mice and may contribute to pathology in this model system.[16]

The lack of a causal link between formation of insoluble aggregates and cell death is reinforced in animal models of HD. For example, the R6/1 and R6/2 transgenic HD mice, which express a mutant htt fragment and present with both nuclear and cytoplasmic aggregates, have behavioural changes consistent with HD but exhibit little neuronal death.[17] These observations support work showing that an early feature of HD is loss of synaptic connections that are independent of neurodegeneration.[18–20] However, it is unclear if the formation and sub-cellular localization of aggregates has a role in this process. Interestingly, 'shortstop' HD mice, which also express a mutant htt fragment, but exhibit primarily nuclear htt aggregates, do not display any clinical signs of neuronal dysfunction or neurodegeneration.[21]

Exocytic trafficking by dendritic recycling endosomes (RE) provides critical components for post-synaptic membrane formation and maintenance.[22] Synaptic components are also retrieved from the plasma membrane by endocytosis into REs and can be either reinserted or degraded.[23] As vesicle trafficking events have been implicated in HD,[24–29] we decided to investigate whether aggregation of a mutant htt exon-1 fragment in the cytoplasm would affect spine maintenance by interfering with endosomal trafficking. Previous reports have shown a disruption of

[1]MRC Toxicology Unit, University of Leicester, Hodgkin Building, Lancaster Road, Leicester, UK; [2]Department of Genetics, University of Leicester, University Road, Leicester, UK and [3]DZNE, German Center for Neurodegenerative Diseases, Ludwig-Erhard-Allee 2, Bonn, Germany
*Corresponding author: P Nicotera, DZNE, German Center for Neurodegenerative Diseases, Ludwig-Erhard Allee 2, Bonn 53175, Germany.
Tel: +49 228 30899x100; E-mail: Pierluigi.Nicotera@DZNE.de
Keywords: Drosophila; neurodegeneration; polyglutamine; synapse; trafficking
Abbreviations: HD, Huntington's disease; polyQ, polyglutamine; htt, huntingtin; RE, recycling endosomes
Received 23.2.10; revised 08.6.10; accepted 10.6.10; Edited by RA Knight; published online 19.11.10

endocytic trafficking in cells expressing a mutant htt fragment,[28,29] which appears to be mediated by Rab11, a GTPase involved in RE function.[30–32] Here, we show that mutant htt expression impairs directional transport from the endocytic recycling centre (ERC) to the plasma membrane in PC12 cells and in the R6/2 HD mouse model. Furthermore, we find that in hippocampal neurons blockage of transport by mutant htt aggregates impairs trafficking of membrane material to dendritic spines, ultimately leading to spine loss. Remarkably, we found that this impairment can be overcome by overexpression of the recycling endosome protein Rab11, and that Rab11 overexpression also rescues HD-relevant phenotypes in a *Drosophila* model of this disease. In total this work suggests that spine loss due to mutant htt aggregates may lead to synaptic loss, and ultimately neuronal dysfunction, in HD and that this impairment can be restored by Rab11.

Results

Endocytic recycling is impaired in a cell culture model of HD. We initially investigated RE activity by monitoring the uptake of Alexa 568-Transferrin (Tfn) into live PC12 cells expressing a GFP-tagged N-terminal htt fragment of htt with either 24 or 74 glutamine repeats (HttQ24-GFP and HttQ72-GFP, respectively) under control of the deoxycline (dox) promoter.[33] Induction of the transgene by 1 μg/ml dox resulted in time-dependent aggregation of mutant htt, with approximately 40% of cells exhibiting aggregates after 4 days (data not shown). In uninduced cells, endocytosed Alexa 568-Tfn was distributed in small puncta; in dox-induced cells, Alexa 568-Tfn was concentrated in large perinuclear bodies with cells expressing HttQ74-GFP (Figure 1a). The kinetics of Alexa 568-Tfn uptake into individual PC12 cells showed that the net rate of uptake

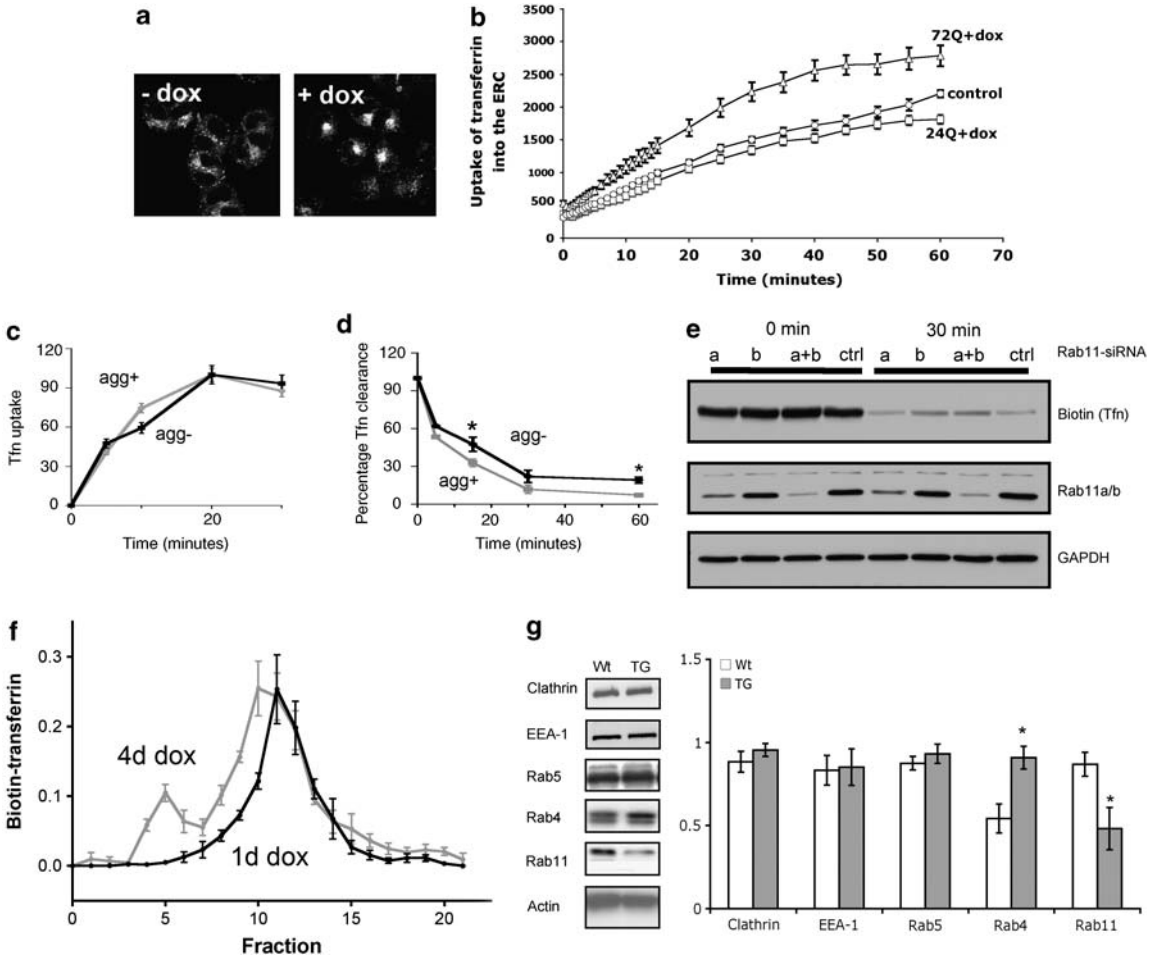

Figure 1 Expression of a mutant htt fragment alters exocytic trafficking in PC12 cells and a mouse model of HD. (**a**) Confocal images of PC12, un-induced and dox-induced showing altered distribution of Tfn after saturation loading. (**b**) Kinetics of net uptake of $Alexa_{568}$-Tfn into PC12 cells with either induction of Htt72Q-GFP for 4 days (triangles), Htt24Q-GFP (squares) or control (untransfected) PC12 cells. Analysis was conducted on at least six cells and the experiment was performed three times; data are mean ± S.E.M. (**c**) Biotin-Tfn uptake into and (**d**) efflux from PC12 cells with (grey) and without (black) Htt74Q-GFP aggregates. Experiment was performed as in Materials and Methods. Data are the mean ± S.E.M. of four determinations. *Efflux significantly lower in aggregate-containing cells, $P<0.05$. (**e**) Rab11 silencing in PC12 cells. Either Rab11a, b or both were silenced and transferrin exit from the cell compared with scrambled control. Lysates were blotted for Tfn, showing reduced clearance in the Rab11b and Rab11 a + b silenced samples after a chase time of 30. (**f**) Analysis of organelles by sucrose density gradient centrifugation. Cells (Htt74Q 1 or 4 days induction) were loaded with biotin transferrin and lysed in 0.32 M sucrose using a ball bearing homogeniser at 4°C. Cell lysates were loaded onto a sucrose gradient (0.45–2 M) and centrifuged for 18 h at 100 000 × *g*. Fractions of 0.5 ml were collected and probed for biotin. (**g**) Proteins from lysates of R6/2 mice and WT litter mates were probed by western blotting ($n=3\pm$ S.E.M) and grouped according to their position in the recycling scheme (*$P<0.05$). EEA-1, early endosomal antigen-1

was greater in PC12 cells expressing HttQ72-GFP (Figure 1b) compared with either untransfected cells or cells expressing a short glutamine repeat. To examine whether this net difference resulted from an increase in endocytosis or a decrease in exocytosis, the total uptake (Figure 1c) and total efflux (Figure 1d) of biotinylated-Tfn was determined separately by western blotting. This revealed impairment in efflux of Tfn from HttQ74-expressing PC12 cells rather than an increased rate of uptake. As Rab11 modulates exit from recycling centres, we tested whether the deficit in Rab11 observed in cells expressing HttQ74-GFP could be because of the impairment in exocytosis. We initially used siRNA oligonucleotides to reduce the level of the two isoforms of Rab11 (a and b) in PC12 cells. Knockdown of either Rab11b alone or Rab11a and b impaired exit from the recycling centre and increased the saturation point for transferrin uptake (Figure 1e). Knockdown of Rab11a alone had no effect on the exit of transferrin from the recycling centre.

Finally, we investigated whether the impaired exit would result in protein accumulation within the recycling centre. Cells were loaded with transferrin and organelles separated by density gradient centrifugation (Figure 1f). This allowed analysis of the recycling centre and associated vesicles. Cells induced for 4 days, a high percentage of which present with aggregates, exhibited an increase in the density of the recycling centre, as well as a pronounced second peak associated with denser vesicles. Strikingly, this data suggests a correlation between mutant htt aggregate load and increased density of the recycling centre.

Levels of proteins involved in endocytic recycling are altered in a mouse model of HD. Next, we looked at the expression levels of a number of proteins involved in endocytic recycling in the R6/2 mice, which are transgenic for an N-terminal fragment of the htt protein containing an expanded glutamine repeat.[34] Proteins involved in endocytosis and early endosome transport (EEA-1, clathrin, Rab5) were unaffected in the R6/2 mouse. However, Rab4, which delivers cargo to the ERC, was significantly increased in the transgenic animals and Rab11, which is involved in exit from the recycling center, was significantly decreased, suggesting an impairment in endocytic recycling. Therefore, our observations in HD model mice support the findings in PC12 cells (Figure 1g).

Loss of dendritic spines in hippocampal neurons occurs at sites of aggregate formation. We next asked whether the decrease in Rab11 and the mutant htt-specific lesion in endocytic recycling could be causally linked to the maintenance of dendritic spines. To this end, we transiently transfected cultures of hippocampal neurons with Htt exon-1 constructs encoding either 25Q or 47Q repeats. After 7 days in culture the cells were simultaneously transfected with the GFP-tagged htt constructs and tdTomato to facilitate the imaging of spine number and morphology. At 7 days post-transfection (14 DIV) neurons showed a uniform expression of HttQ25-GFP, distributed in a similar pattern to that of tdTomato (Figure 2a). In contrast, we saw a spectrum of HttQ47-GFP distribution with 24% of the cells having accumulations of GFP (often sitting under spines) (Figure 2c), 42% showing discrete, highly fluorescent aggregates (Figure 2d), and 34% in which GFP expression was diffused (Figure 2b). We quantified the number of dendritic protrusions in areas of cells showing these three types of HttQ47-GFP morphology, as well as in HttQ25-GFP cells. This revealed a significant decrease in the total spine number in cells where there was an accumulation of HttQ47-GFP compared with either HttQ25 cells or HttQ47 cells with diffuse GFP fluorescence (Figure 2e). To test if aggregate formation influenced spine density we counted spine number within 10 μm (either side) of an aggregate and compared it with dendritic areas distant from aggregates in the same HttQ47-expressing neuron (Figure 2f). This revealed fewer dendritic spines near to aggregate formation (Figure 2g). Furthermore, spine loss was symmetrical about the aggregate and not biased to distal or proximal sides, relative to the neuronal soma, suggesting that aggregates do not physically block vesicular transport.

Mushroom-type dendritic spines are selectively lost in the vicinity of aggregates. Mushroom-type spines are considered to be the most mature form in hippocampal neurons and contain abundant glutamate receptors (GluR) compared with filipodia (Matsuzaki *et al*., 2001). Individual quantification of the three spine types – filopodia, stubby and mushroom revealed that mushroom spines are selectively decreased in the vicinity of aggregates in HttQ47-GFP-expressing neurons compared with HttQ25-GFP (Figure 2h). The selective loss of mushroom spines was progressive; with 21 DIV neurons showing a greater percentage loss of mushroom spines than those at 14 DIV (Figure 2i). In this time period mushroom spine density increases by 1.9-fold in HttQ25-GFP-expressing neurons but remains unchanged ($P=0.63$; Student's *t*-test) in HttQ47-GFP-expressing cells, showing the effect is not transient nor a result of delaying spine development.

Exocytic trafficking is impaired by htt aggregates. To explore the possibility that the above spine loss resulted from impaired exocytic trafficking, we loaded Alexa 633-Tfn in HttQ47-GFP-expressing hippocampal neurons. We found that in the vicinity of dendritic HttQ47 aggregates, Tfn-containing vesicle volume was increased (Figure 3a). Moreover, some endocytosed Alexa 633-Tfn appeared to localise around dendritic aggregates of HttQ47-GFP (Figure 3b).

Next, we investigated the effects of dendritic aggregates on GluR recycling. GluRs are stored in dendritic REs and transported to the postsynaptic density upon stimulation.[35] We focused on dendritic areas adjacent to mushroom-spines in HttQ25-GFP- and HttQ47-GFP-expressing hippocampal neurons and determined the distribution of GluR1 between the spine and the underlying dendrite (Figure 3c). In neurons containing HttQ47-GFP aggregates a higher proportion of GluR1 were retained within dendrites and not transported into spines (Figure 3d). Furthermore, we observed GluR1 staining in the vicinity of protein inclusions (Figure 3e).

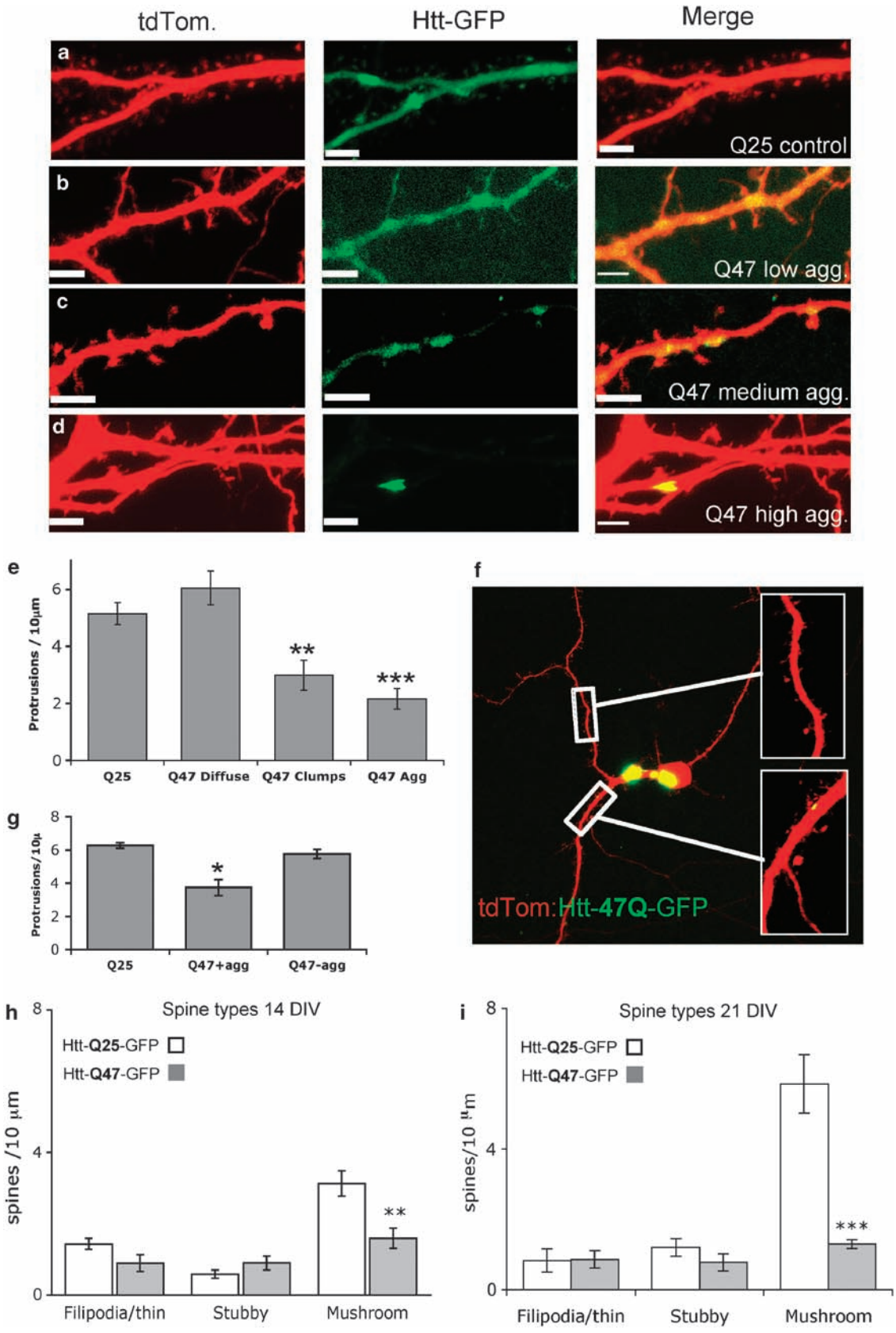
tdTom.
Htt-GFP
Merge
a
b
c
d
Q25 control
Q47 low agg.
Q47 medium agg.
Q47 high agg.
e
Protrusions / 10µm
0
2
4
6
**
***
Q25
Q47 Diffuse
Q47 Clumps
Q47 Agg
f
tdTom:Htt-47Q-GFP
g
Protrusions/10µ
0
2
4
6
8
*
Q25
Q47+agg
Q47-agg
h
Spine types 14 DIV
Htt-Q25-GFP
Htt-Q47-GFP
spines /10 µm
0
4
8
**
Filipodia/thin
Stubby
Mushroom
i
Spine types 21 DIV
Htt-Q25-GFP
Htt-Q47-GFP
spines/10 µm
0
4
8
***
Filipodia/thin
Stubby
Mushroom

Enlarged amphisome-like structures form around mutant htt aggregates in dystrophic dendrites. As the small GTPase Rab11 is essential both for exocytic trafficking from REs and for amphisome formation by fusion of multivesicular bodies (MVBs) with autophagosomes,[36] we investigated trafficking organelles involved in the recycling and degradation pathways. In dendrites of neurons co-transfected with Rab11-EYFP, Rab11 distribution changed from diffuse dendritic staining in HttQ25-GFP-expressing neurons to punctuate clustering around protein aggregates in those expressing HttQ47-GFP (Figures 4a and b). Many of the dendritic regions around these HttQ47-GFP aggregates were dystrophic and contained vacuolar swellings (Figures 4c and e), which were also positive for the autophagic marker, LC3-mRFP (Figure 4d). Close association of Rab11 with aggregates could also be associated with amphisome-like structures.[37,38] We examined this question by triply transfecting neurons with Rab11-EYFP, HttQ47-GFP and LC3-mRFP and observed a large LC3-positive structures in the dystrophic swellings that are associated with aggregates (Figures 4c and d, f–h). The LC3-positive structures contained both HttQ47-GFP aggregates and Rab11,

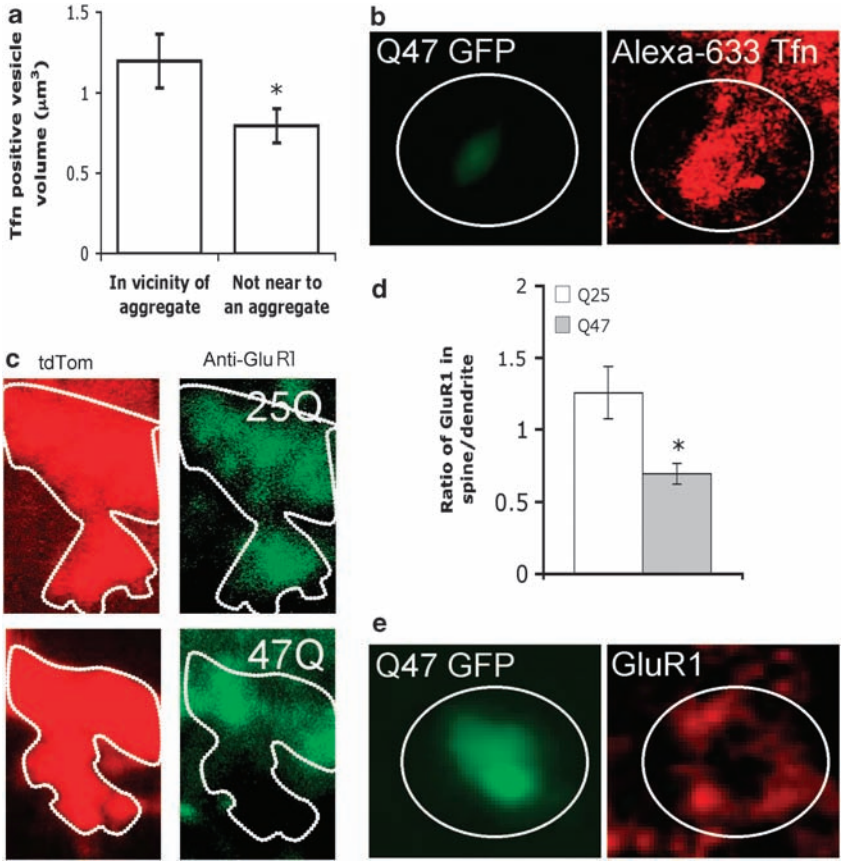

Figure 3 Dendritic HttQ47 aggregates impair endocytic recycling. **(a)** HttQ47-GFP-expressing neurons were loaded with Alexa633-Tfn for 1 h, fixed and imaged by confocal microscopy. Volocity software was used to calculate the volume of the Tfn-containing vesicles in the dendrites. The relative volumes were measured in areas close (10 μm) to an aggregate and in dendritic regions with no visible aggregates. Data are the mean ± S.E.M. of 29 determinations. *Significantly different; $P<0.05$. (**b**) Endocytosed Tfn accumulates in the vicinity of dendritic HttQ47-GFP aggregates. (**c**) Fixed, permeabilised HttQ47-GFP- and HttQ25-GFP-expressing neurons, both co-expressing tdTomato, were stained for GluR1. Note absence of GluR1 in spine of HttQ47-expressing neuron (**d**). Ratio of spine/dendrite GluR1 in HttQ25-GFP and HttQ47-GFP neurons. Data are mean ± S.E.M. of 13 determinations; *Significantly different, $P<0.05$). (**e**) GluR1 localises around dendritic HttQ47-GFP aggregates

Figure 2 Localised loss of mushroom spines close to dendritic HttQ47 aggregates. (**a**) Distribution of HttQ25-GFP and tdTomato (cell fill) in the dendritic region of a mouse hippocampal neuron (14 DIV). (**b**) HttQ47-GFP-expressing cell (14 DIV) showing diffuse morphology of GFP expression. (**c**) A separate HttQ47-GFP-expressing cell showing 'clumping' of GFP; note the proximity of the clumps of GFP to dendritic spines. (**d**) An HttQ47-GFP-expressing cell containing a highly fluorescent dendritic aggregate. (**e**) A reduced number of total protrusions seen in dendritic regions of cells containing clumps and aggregates of HttQ47-GFP compared with HttQ25-GFP-expressing cells. Data are mean ± S.E.M. of 11 determinations; $^{**}P<0.01$; $^{***}P<0.001$. (**f**) An HttQ47-GFP-expressing cell showing dendritic regions with (bottom inset) and without (top inset) aggregates. (**g**) Reduced numbers of spines within 10 μm of an aggregate (Q47 + agg) in HttQ47-GFP-expressing neurons compared with numbers in aggregate-free areas (Q47-agg) or in dendrites of HttQ25-GFP-expressing neurons. Data are mean ± S.E.M. of 20 determinations; $^{*}P<0.05$. (**h**) Different spine types (filipodia/thin, stubby and mushroom were quantified in the vicinity of aggregates (up to 40 μm stretch of dendrite containing a discrete aggregate or aggregates) or in corresponding areas in HttQ25-expressing cells (mean ± S.E.M.). At least 15 cells were used for each calculation from several different preparations $^{**}P<0.01$. Cells were transfected after seven DIV and imaged 7 days later. (**i**) Spine morphology in cultures transfected after seven DIV and imaged 14 days later (mean ± S.E.M.; $^{***}P<0.0001$ two-way ANOVA)

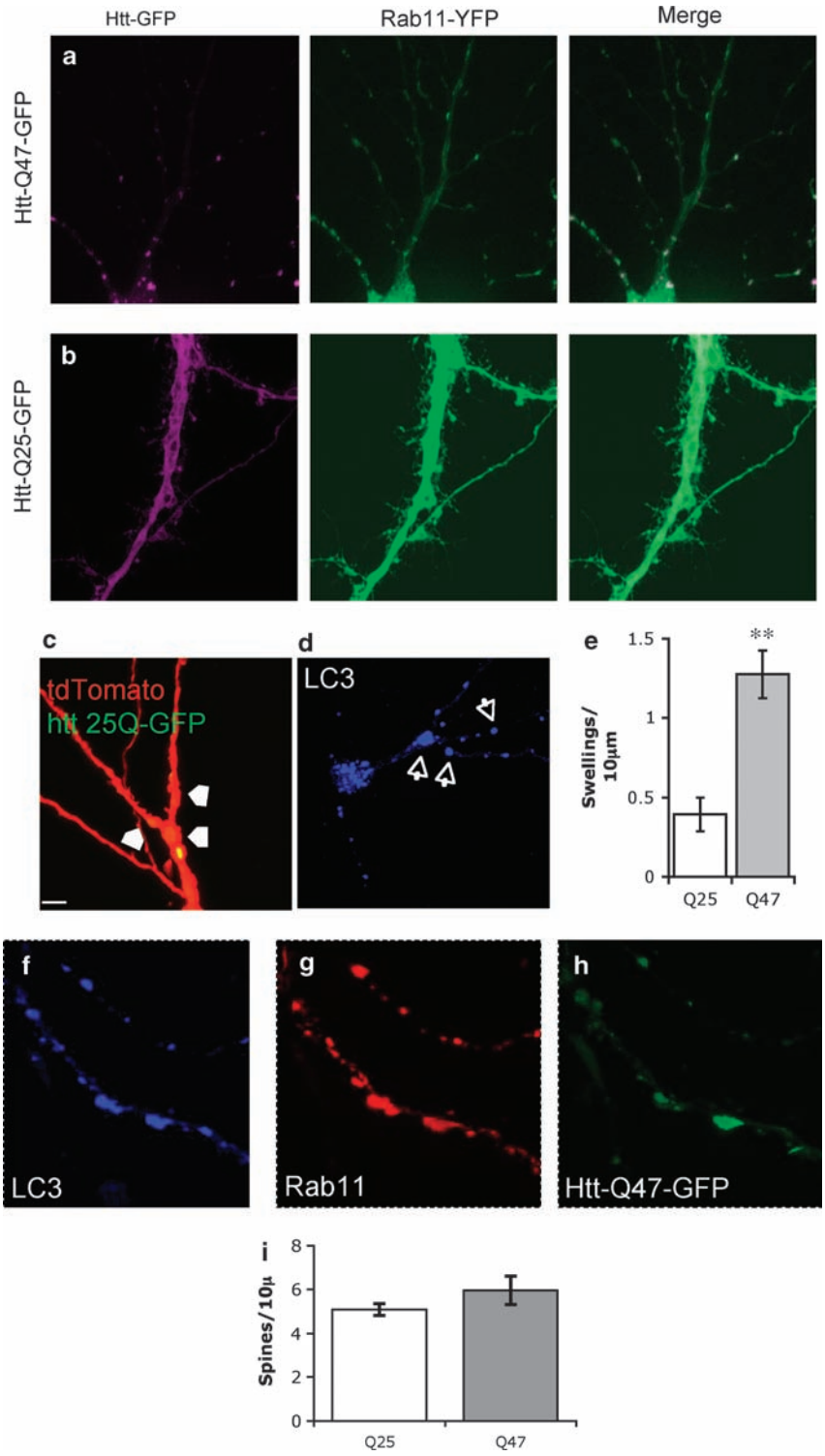

Figure 4 Altered Rab11 distribution and autophagosomal markers are associated with HttQ47 aggregates in dystrophic dendrites. Neurons were co-transfected with Rab11-YFP and either HttQ47-GFP (**a**) or HttQ25-GFP (**b**). Spectral unmixing was used to resolve the YFP and GFP signals. Co-localization of Rab11 and HttQ47 aggregates is seen as bright puncta in the dendrites. (**c**) Dystrophic swelling (arrows) in HttQ47-GFP cells co-transfected with tdTomato: these swellings were also associated with LC3 accumulation (**d**). (**e**) Numbers of dystrophic swellings were quantified in HttQ47-GFP- and HttQ25-GFP-expressing neurons. Data are mean ± S.E.M. of 15 determinations; **Significantly different, $P<0.01$). Neurons triply transfected with Htt- LC3-mRFP (**f**), Rab11-YFP (**g**) and HttQ47-GFP (**h**) were imaged and spectrally unmixed to resolve the GFP/YFP signals and subsequently re-imaged to visualise the LC3-mRFP. The images show the LC3, Rab11 and HttQ47 signals associate in the same dendritic areas. (**i**) Numbers of spines within 10 μm of an aggregate in HttQ47-GFP-expressing neurons co-transfected with Rab11 compared with numbers in HttQ25-GFP showed no difference

therefore defining them as amphisomes. We counted spine number in cells co-transfected with either Rab11-EYFP and HttQ47-GFP or HttQ47GFP and HttQ25GFP, and in contrast to Figure 2g there was no significant difference between spine densities in HttQ47-GFP aggregate-containing regions and HttQ25-GFP-expressing cells (Figure 4i). This demonstrates rescue of phenotype by overexpression of Rab11in hippocampal neurons.

Rab11 overexpression rescues disease-relevant pathology in HD flies. To address whether Rab11 overexpression can ameliorate HD-relevant phenotypes *in vivo*, we took advantage of a widely used *Drosophila* HD model that expresses a human htt exon-1 fragment similar to that expressed in *R6/2* HD model mice (1). Mutant htt transgene (HttQ93) expression was driven pan-neuronally using the *UAS/GAL4* system, generating several phenotypes, including neurodegeneration of photoreceptor cells (rhabdomeres) in the fly eye, decreased adult emergence from the pupal case (eclosion) and decreased lifespan/survival (1). We therefore analysed the level of neurodegeneration in flies expressing HttQ93 pan-neurally using the *elavgal4* driver, and compared them with those expressing both HttQ93 and Rab11. We found that overexpressing Rab11 in this way gives a highly significant ~43% rescue of rhabdomere degeneration at day 1 after eclosion (Figures 5a and b). Next, we measured the frequency of eclosion in HD flies with or without overexpression of Rab11. Previous studies determined that ~20–30% of flies expressing HttQ93 emerge from the pupal case.[39,40] Similarly, in our experiments, we observed that ~40% of HD flies emerged as adults (Figure 5c). Remarkably, we found that overexpression of Rab11 almost completely rescued the HD eclosion phenotype, with a greater than twofold increase in emergence (Figure 5c). HD flies that are able to eclose have reduced adult survival. In order to determine if Rab11 overexpression is able to rescue this phenotype, we performed survival analysis on Rab11 HD flies and HD flies alone. Provocatively, we found that overexpression of Rab11 increased median survival of HD flies by 50%, from 10 to 15 days (Figure 5d). In total, these results reveal for the first time that Rab11 overexpression rescues several disease-relevant phenotypes in an animal model of HD. This *in vivo* model confirms the role of endocytic trafficking in the pathology of HD.

Discussion

Synaptic loss has been observed in HD transgenic mice along with a high aggregate load in the neuropil.[20,41] Recently, it has been shown that reducing the levels of htt aggregates in the neuropil of HD transgenic mice ameliorates neurological phenotypes.[42] We developed a cellular HD model in primary hippocampal neurons to allow examination of dendritic spines in the presence of mutant htt exon-1 fragment aggregates. In this model, we observed fewer dendritic spines close to htt aggregates but not in areas where the mutant protein was still diffuse and soluble. These areas of aggregate formation were also associated with two other phenomena: a rearrangement of the endocytic recycling network and enlarged autophagic vacuoles. It is well established that protein aggregates are refractory to digestion and reside in autolytic compartments.[3,43,44] Our results suggest that an early consequence of reduced clearance is loss of dendritic spines.

Our data reveal a lesion in endocytic recycling induced by aggregate formation. The multivesicular body is critical for the autophagic clearance of protein aggregates[45]and dendrites have MVBs in close proximity to dendritic spines and REs.[46] The MVB is a late endocytic trafficking vesicle containing a number of internal vesicles of low pH that facilitate proteolysis, which fuse with autophagosomes in a Rab11-dependent step to form a hybrid organelle; the amphisome.[36,38] In the final stage, amphisomes fuse with lysosomes to generate autolysosomes that degrade susceptible cargo.

Rab11 also has a general role in the exocytic trafficking of membrane from dendritic REs to the dendritic spine. Therefore, material accumulating in degradative vesicles could appropriate Rab11, compromising the effectiveness of exit from the RE: this becomes particularly critical if Rab11 is present in limiting quantities. We show here that enlarged amphisome-like structures, formed from the Rab11-dependent fusion of MVBs with LC3-positive autophagosomes, are associated with areas of dendritic dystrophy and reduced spine number. We suggest that redistribution of Rab11 to the amphisome impairs Rab11-dependent exocytosis from the RE. In support of a central role for Rab11 in the mechanism of aggregate formation and synaptic loss, overexpression of Rab11 along with HttQ47-GFP prevented spine loss and aggregate formation. Finally, we have shown that overexpression of Rab11 in a *Drosophila* model of HD can rescue several disease-relevant phenotypes, including survival and neurodegeneration, which further supports a central role for impairment of Rab11 function in HD pathology, and may inform future therapeutic strategies for this disorder. In total, this work suggests that impairment of Rab11-dependent exocytosis may have a role in the progressive loss of synaptic connectivity in HD. It is possible that similar mechanisms could be occuring in other slow neurodegenerative diseases where protein aggregates are a hallmark of pathology.

Materials and Methods

Tissue culture and transfection with plasmids. Primary hippocampal cultures were prepared from 1-day-old rats as described previously.[47] Mouse hippocampal neurons were prepared from 1-day-old C57/BL6 neonates in a similar manner to the rat cultures, except that mouse neurons were grown in Neurobasal A medium supplemented with 2% B27, 2 mM glutamax and 1 mg/ml gentamicin. At 7 DIV, neurons were transfected with plasmids expressing tdTomato, HttQ25-GFP, HttQ47-GFP, Rab11-EYFP and LC3-mRFP. A volume of 1 μg DNA and 0.5 μl Lipofectamine 2000 (Invitrogen, Paisley, UK) was added to cells for 6 h, before medium was replaced. Where HttQ25-GFP and HttQ47-GFP constructs were used in conjunction with tdTomato (Clontech-Takara Bio Europe, Saint-Germain-en-Laye, France), a DNA ratio of 0.67 μg Htt-GFP to 0.33 μg tdTomato was used. For triple transfection, equal amounts of all three constructs were used. Neurons were imaged between 14 and 21 DIV. PC12 cells expressing HttQ74-GFP or HttQ25-GFP under control of a tetracycline promoter were grown and induced as described previously.[33] All htt constructs encode N-terminal htt exon-1 fragments with polyQ lengths as indicated.

Confocal imaging and analysis. Cells were mounted on a Zeiss LSM 510 META laser scanning confocal microscope and imaged at 37 °C in Krebs buffer. In general, a series of z-slices were obtained and used to reconstruct a 3D model of the dendritic region of interest using Volocity software (Improvision; PerkinElmer, Cambridgeshire, UK) to identify spine morphology. For live cell imaging of

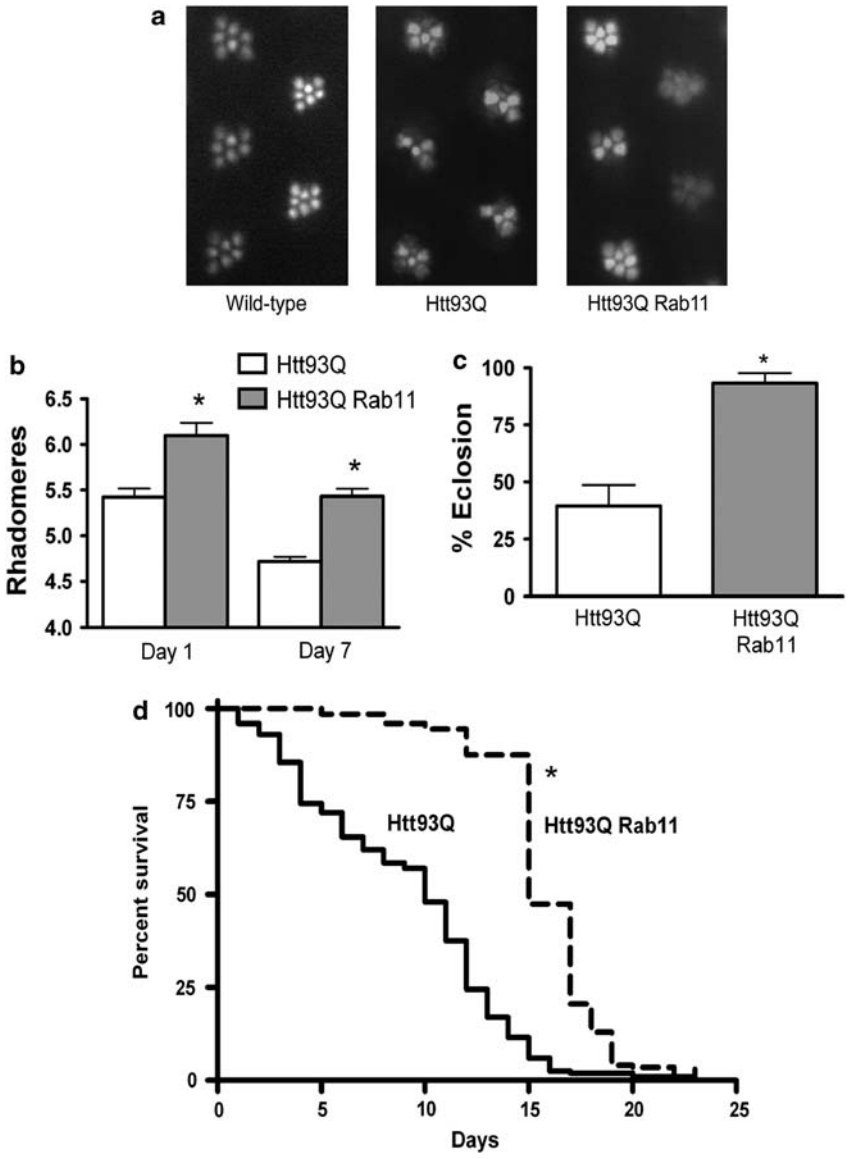

Figure 5 Overexpression of Rab11 rescues disease-relevant phenotypes in HD flies. (**a**) Neurodegeneration of rhabdomeres is partially rescued in HD flies expressing Rab11. Pseudopupil images from wild type, HD flies and HD flies overexpressing Rab11 at day 7. In wild-type flies, seven rhabdomeres are visible per ommatidium. (**b**) Quantification of average rhabdomeres per ommatidum in HD flies with and without pan-neural Rab11 overexpression at day 1 and day 7 after eclosion. Significant genotype ($F_{1,46} = 55.03$ $P \ll 0.0001$) and Age ($F_{1,46} = 54.26$, $P \ll 0.0001$), effects were observed, with no interaction. At day 1 $\sim$43% rescue of neurodegeneration was observed, whereas at day 7 $\sim$30% rescue was observed. (**c**) Rab11 overexpression rescues HD adult emergence. Segregating crosses were set up to generate Htt93Q Rab11 expressing females and control males that carried the two *UAS* transgenes but not the *elavgal4* driver. Eclosion percentage was calculated by dividing the number of females by the total number of flies that emerged per vial. Eclosion was almost completely rescued in the Rab11 flies ($^*P < 0.0001$). HD flies $n = 1076$; HD Rab11 flies $n = 2626$. (**d**) Rab 11 overexpression increased median survival of adult HD flies. The number of flies surviving from each cohort was determined every 2 days. Htt93Q flies overexpressing Rab11 (dashed line) were significantly different from those expressing Htt93Q alone ($^*P < 0.0001$). $n = 200$ animals per genotype

transferrin uptake, PC12 cells were initially washed with serum-free medium (SFM) and incubated for 30 min at 37°C to clear the cells of transferrin. The cells were then mounted onto the microscope and transferrin-Alexa-633 was added (final concentration 5 μg/ml). The time lapse was immediately started and run for 1 h at room temperature. Z-Stacks of nine images were taken at each time point, starting at an interval of 30 s and finishing with an interval of 5 min. To simultaneously image YFP and GFP signals in transfected hippocampal cells, emission fingerprinting was used. Essentially, spectra from either YFP or GFP transfected Hela cells were used to derive fingerprints, that was subsequently used to unmix signals from doubly transfected cells.

Analysis of transferrin uptake and extrusion from PC12 cells. PC12 cells were washed twice with warm SFM and incubated for 1 h at 37°C to clear them of transferrin. To measure uptake, cells were loaded with 2 μg/ml biotinylated transferrin in SFM at room temperature for 5, 10, 20 or 30 min. At each time point, the cell culture plate was cooled on ice; the cells were washed twice with cold PBS and lysed in RIPA buffer. Proteins were resolved by SDS-PAGE, blotted and probed with an HRP-conjugated antibody to biotin. To measure transferrin extrusion, cells cleared of unlabelled transferrin were loaded with biotinylated transferrin (10 μg/ml) in SFM for 1 h at 37°C. After loading, the cells were quickly washed twice in pre-warmed SFM and then chased for 0, 15, 30 and 60 min in

pre-warmed serum-containing medium. At each time point, the cells were harvested and processed as for the uptake experiment.

Immunocytochemistry. Hippocampal neurons were fixed in 4% paraformaldehyde and permeabilised in 0.1% Triton. After subsequent overnight blocking in 0.5% BSA, 0.2% goat serum in PBS, cells were incubated with anti-GluR1 (Millipore; AB1504, Watford, UK) at a dilution of 1 : 100 in blocking buffer. Cells were washed and incubated with a secondary antibody (Alexa-633 conjugated; Invitrogen) and mounted.

Fly stocks. Flies were raised on maize media, in LD12 : 12 at 25°C. The chromosomal *elav-GAL4* (c155) driver and the *w;UASRab11-GFP* (8506) stocks were obtained from the Bloomington Stock Centre, University of Indiana, Bloomington, IN, USA. The *w;+;UAS Htt* exon-1-Q93 flies have been previously described (line P463[39]). Experimental flies were: *Htt = w,elavGAL4/w;+;UASHtt/+* and *HttRab11 = w,elavGAL4/w; UASRab11/+; UASHtt/+*.

Eclosion analysis. Males carring the pan-neuronal *elavGAL4* driver on the X chromosome were crossed to virgin females homozygous for the UAS-transgene(s). Of the resulting progeny, only females inherited the *elavGAL4* driver and therefore expressed the UAS-transgene(s), whereas males carried the UAS-transgenes but not the driver. The numbers of females and males eclosing in each vial were counted every day until all the F1 progeny had emerged. Percent eclosion was calculated as (no. of females/no. of males) $\times$ 100. For statistical analysis two-way ANOVA was used to compare the proportion of *HttRab11* females eclosing per vial with that of *Htt* males from their corresponding crosses ($F = 40.4_{1,30}$ $P < < 0.0001$). More than 1000 progeny were counted for each cross.

Survival analysis. *Htt* and *HttRab11* females were generated as described above, and collected within 24 h from eclosion. A total of 600 *Htt* and 200 *HttRab11* flies were kept at 25°C in groups of 10 per vial. Every other day the number of surviving flies was scored in each vial, and the flies moved to fresh food. Survival statistics were performed using Kaplan–Meier survival curve analysis with log rank test.

Pseudopupil analysis. The number of visible rhabdomeres per ommatidium was scored[39] for >100 ommatidia per fly, and at least 10 flies were examined per genotype. The two-way ANOVA was used for statistical analysis.

Conflict of Interest

The authors declare no conflict of interest.

Acknowledgements. We thank Maria Guerra-Martin for assistance with neuronal cell cultures. We would like to thank David Rubinsztein for the mutant htt expressing PC12 cell-lines, Marino Zerial for the Rab11EYFP construct, Edward Bampton for the LC3-mRFP construct and Jenny Morton for tissue from R6/2 mice. The FLAG-tagged tdTomato construct was kindly provided by Michael J Schell. We would also like to thank Larry Marsh, Leslie Thompson, and Judit Pallos for the HttQ93 exon 1 fly lines, and for critical advice and suggestions in the study of these animals. Finally, we thank Ian Forsythe and Paul Muchowski for general advice, discussion and critical reading of the manuscript.

1. Mangiarini L, Sathasivam K, Seller M, Cozens B, Harper A, Hetherington C *et al.* Exon 1 of the HD gene with an expanded CAG repeat is sufficient to cause a progressive neurological phenotype in transgenic mice. *Cell* 1996; **87**: 493–506.
2. Scherzinger E, Lurz R, Turmaine M, Mangiarini L, Hollenbach B, Hasenbank R *et al.* Huntingtin-encoded polyglutamine expansions form amyloid-like protein aggregates *in vitro* and *in vivo*. *Cell* 1997; **90**: 549–558.
3. DiFiglia M, Sapp E, Chase KO, Davies SW, Bates GP, Vonsattel JP *et al.* Aggregation of huntingtin in neuronal intranuclear inclusions and dystrophic neurites in brain. *Science* 1997; **277**: 1990–1993.
4. Davies SW, Turmaine M, Cozens BA, DiFiglia M, Sharp AH, Ross CA *et al.* Formation of neuronal intranuclear inclusions underlies the neurological dysfunction in mice transgenic for the HD mutation. *Cell* 1997; **90**: 537–548.
5. Scherzinger E, Sittler A, Schweiger K, Heiser V, Lurz R, Hasenbank R *et al.* Self-assembly of polyglutamine-containing huntingtin fragments into amyloid-like fibrils: implications for Huntington's disease pathology. *Proc Natl Acad Sci USA* 1999; **96**: 4604–4609.
6. Chen S, Ferrone FA, Wetzel R. Huntington's disease age-of-onset linked to polyglutamine aggregation nucleation. *Proc Natl Acad Sci USA* 2002; **99**: 11884–11889.
7. Alves-Rodrigues A, Gregori L, Figueiredo-Pereira ME. Ubiquitin, cellular inclusions and their role in neurodegeneration. *Trends Neurosci* 1998; **21**: 516–520.
8. Chai Y, Wu L, Griffin JD, Paulson HL. The role of protein composition in specifying nuclear inclusion formation in polyglutamine disease. *J Biol Chem* 2001; **276**: 44889–44897.
9. Bucciantini M, Giannoni E, Chiti F, Baroni F, Formigli L, Zurdo J *et al.* Inherent toxicity of aggregates implies a common mechanism for protein misfolding diseases. *Nature* 2002; **416**: 507–511.
10. Carmichael J, Chatellier J, Woolfson A, Milstein C, Fersht AR, Rubinsztein DC. Bacterial and yeast chaperones reduce both aggregate formation and cell death in mammalian cell models of Huntington's disease. *Proc Natl Acad Sci USA* 2000; **97**: 9701–9705.
11. Saudou F, Finkbeiner S, Devys D, Greenberg ME. Huntingtin acts in the nucleus to induce apoptosis but death does not correlate with the formation of intranuclear inclusions. *Cell* 1998; **95**: 55–66.
12. Tagawa K, Hoshino M, Okuda T, Ueda H, Hayashi H, Engemann S *et al.* Distinct aggregation and cell death patterns among different types of primary neurons induced by mutant huntingtin protein. *J Neurochem* 2004; **89**: 974–987.
13. Giorgini F, Guidetti P, Nguyen Q, Bennett SC, Muchowski PJ. A genomic screen in yeast implicates kynurenine 3-monooxygenase as a therapeutic target for Huntington disease. *Nat Genet* 2005; **37**: 526–531.
14. Arrasate M, Mitra S, Schweitzer ES, Segal MR, Finkbeiner S. Inclusion body formation reduces levels of mutant huntingtin and the risk of neuronal death. *Nature* 2004; **431**: 805–810.
15. Legleiter J, Mitchell E, Lotz GP, Sapp E, Ng C, Difiglia M *et al.* Mutant Huntingtin fragments form oligomers in a polyglutamine length-dependent manner *in vitro* and *in vivo*. *J Biol Chem* 2010; **285**: 14777–14790.
16. Weiss A, Klein C, Woodman B, Sathasivam K, Bibel M, Regulier E *et al.* Sensitive biochemical aggregate detection reveals aggregation onset before symptom development in cellular and murine models of Huntington's disease. *J Neurochem* 2008; **104**: 846–858.
17. Martin-Aparicio E, Yamamoto A, Hernandez F, Hen R, Avila J, Lucas JJ. Proteasomal-dependent aggregate reversal and absence of cell death in a conditional mouse model of Huntington's disease. *J Neurosci* 2001; **21**: 8772–8781.
18. Lee JA, Lim CS, Lee SH, Kim H, Nukina N, Kaang BK. Aggregate formation and the impairment of long-term synaptic facilitation by ectopic expression of mutant huntingtin in Aplysia neurons. *J Neurochem* 2003; **85**: 160–169.
19. Li H, Li SH, Cheng AL, Mangiarini L, Bates GP, Li XJ. Ultrastructural localization and progressive formation of neuropil aggregates in Huntington's disease transgenic mice. *Hum Mol Genet* 1999; **8**: 1227–1236.
20. Gutekunst CA, Li SH, Yi H, Mulroy JS, Kuemmerle S, Jones R *et al.* Nuclear and neuropil aggregates in Huntington's disease: relationship to neuropathology. *J Neurosci* 1999; **19**: 2522–2534.
21. Slow EJ, Graham RK, Osmand AP, Devon RS, Lu G, Deng Y *et al.* Absence of behavioral abnormalities and neurodegeneration *in vivo* despite widespread neuronal huntingtin inclusions. *Proc Natl Acad Sci USA* 2005; **102**: 11402–11407.
22. Park M, Salgado JM, Ostroff L, Helton TD, Robinson CG, Harris KM *et al.* Plasticity-induced growth of dendritic spines by exocytic trafficking from recycling endosomes. *Neuron* 2006; **52**: 817–830.
23. Ehlers MD. Reinsertion or degradation of AMPA receptors determined by activity-dependent endocytic sorting. *Neuron* 2000; **28**: 511–525.
24. Li Y, Chin LS, Levey AI, Li L. Huntingtin-associated protein 1 interacts with hepatocyte growth factor-regulated tyrosine kinase substrate and functions in endosomal trafficking. *J Biol Chem* 2002; **277**: 28212–28221.
25. Qin ZH, Wang Y, Sapp E, Cuiffo B, Wanker E, Hayden MR *et al.* Huntingtin bodies sequester vesicle-associated proteins by a polyproline-dependent interaction. *J Neurosci* 2004; **24**: 269–281.
26. Trushina E, Dyer RB, Badger II JD, Ure D, Eide L, Tran DD *et al.* Mutant huntingtin impairs axonal trafficking in mammalian neurons *in vivo* and *in vitro*. *Mol Cell Biol* 2004; **24**: 8195–8209.
27. Pal A, Severin F, Hopfner S, Zerial M. Regulation of endosome dynamics by Rab5 and Huntingtin-HAP40 effector complex in physiological *versus* pathological conditions. *Methods Enzymol* 2008; **438**: 239–257.
28. Li X, Standley C, Sapp E, Valencia A, Qin ZH, Kegel KB *et al.* Mutant huntingtin impairs vesicle formation from recycling endosomes by interfering with Rab11 activity. *Mol Cell Biol* 2009; **29**: 6106–6116.
29. Li X, Sapp E, Chase K, Comer-Tierney LA, Masso N, Alexander J *et al.* Disruption of Rab11 activity in a knock-in mouse model of Huntington's disease. *Neurobiol Dis* 2009; **36**: 374–383.
30. Ullrich O, Reinsch S, Urbe S, Zerial M, Parton RG. Rab11 regulates recycling through the pericentriolar recycling endosome. *J Cell Biol* 1996; **135**: 913–924.
31. Hales CM, Vaerman JP, Goldenring JR. Rab11 family interacting protein 2 associates with Myosin Vb and regulates plasma membrane recycling. *J Biol Chem* 2002; **277**: 50415–50421.
32. Wilcke M, Johannes L, Galli T, Mayau V, Goud B, Salamero J. Rab11 regulates the compartmentalization of early endosomes required for efficient transport from early endosomes to the trans-golgi network. *J Cell Biol* 2000; **151**: 1207–1220.

33. Wyttenbach A, Swartz J, Kita H, Thykjaer T, Carmichael J, Bradley J *et al.* Polyglutamine expansions cause decreased CRE-mediated transcription and early gene expression changes prior to cell death in an inducible cell model of Huntington's disease. *Hum Mol Genet* 2001; **10**: 1829–1845.
34. Carter RJ, Lione LA, Humby T, Mangiarini L, Mahal A, Bates GP *et al.* Characterization of progressive motor deficits in mice transgenic for the human Huntington′s disease mutation. *J Neurosci* 1999; **19**: 3248–3257.
35. Park M, Penick EC, Edwards JG, Kauer JA, Ehlers MD. Recycling endosomes supply AMPA receptors for LTP. *Science* 2004; **305**: 1972–1975.
36. Fader CM, Colombo MI. Autophagy and multivesicular bodies: two closely related partners. *Cell Death Differ* 2009; **16**: 70–78.
37. Berg TO, Fengsrud M, Stromhaug PE, Berg T, Seglen PO. Isolation and characterization of rat liver amphisomes. Evidence for fusion of autophagosomes with both early and late endosomes. *J Biol Chem* 1998; **273**: 21883–21892.
38. Fader CM, Sanchez D, Furlan M, Colombo MI. Induction of autophagy promotes fusion of multivesicular bodies with autophagic vacuoles in k562 cells. *Traffic* 2008; **9**: 230–250.
39. Steffan JS, Bodai L, Pallos J, Poelman M, McCampbell A, Apostol BL *et al.* Histone deacetylase inhibitors arrest polyglutamine-dependent neurodegeneration in Drosophila. *Nature* 2001; **413**: 739–743.
40. Wolfgang WJ, Miller TW, Webster JM, Huston JS, Thompson LM, Marsh JL *et al.* Suppression of Huntington's disease pathology in Drosophila by human single-chain Fv antibodies. *Proc Natl Acad Sci USA* 2005; **102**: 11563–11568.
41. DiProspero NA, Chen EY, Charles V, Plomann M, Kordower JH, Tagle DA. Early changes in Huntington's disease patient brains involve alterations in cytoskeletal and synaptic elements. *J Neurocytol* 2004; **33**: 517–533.
42. Wang CE, Zhou H, McGuire JR, Cerullo V, Lee B, Li SH *et al.* Suppression of neuropil aggregates and neurological symptoms by an intracellular antibody implicates the cytoplasmic toxicity of mutant huntingtin. *J Cell Biol* 2008; **181**: 803–816.
43. Waelter S, Boeddrich A, Lurz R, Scherzinger E, Lueder G, Lehrach H *et al.* Accumulation of mutant huntingtin fragments in aggresome-like inclusion bodies as a result of insufficient protein degradation. *Mol Biol Cell* 2001; **12**: 1393–1407.
44. Verhoef LG, Lindsten K, Masucci MG, Dantuma NP. Aggregate formation inhibits proteasomal degradation of polyglutamine proteins. *Hum Mol Genet* 2002; **11**: 2689–2700.
45. Filimonenko M, Stuffers S, Raiborg C, Yamamoto A, Malerod L, Fisher EM *et al.* Functional multivesicular bodies are required for autophagic clearance of protein aggregates associated with neurodegenerative disease. *J Cell Biol* 2007; **179**: 485–500.
46. Cooney JR, Hurlburt JL, Selig DK, Harris KM, Fiala JC. Endosomal compartments serve multiple hippocampal dendritic spines from a widespread rather than a local store of recycling membrane. *J Neurosci* 2002; **22**: 2215–2224.
47. Young KW, Billups D, Nelson CP, Johnston N, Willets JM, Schell MJ *et al.* Muscarinic acetylcholine receptor activation enhances hippocampal neuron excitability and potentiates synaptically evoked Ca(2+) signals via phosphatidylinositol 4,5-bisphosphate depletion. *Mol Cell Neurosci* 2005; **30**: 48–57.